BRAIN
A JOURNAL OF NEUROLOGY

Spreading depolarizations cycle around and enlarge focal ischaemic brain lesions

Hajime Nakamura,[1,2,]* Anthony J. Strong,[3,]* Christian Dohmen,[1,4,]* Oliver W. Sakowitz,[5] Stefan Vollmar,[1] Michael Sué,[1] Lutz Kracht,[1] Parastoo Hashemi,[6] Robin Bhatia,[3] Toshiki Yoshimine,[2] Jens P. Dreier,[7,8] Andrew K. Dunn[9] and Rudolf Graf[1]

1 Max Planck Institute for Neurological Research, 50931 Cologne, Germany
2 Department of Neurosurgery, Osaka University Graduate School of Medicine, 2-2 Yamadaoka, Japan
3 Department of Clinical Neuroscience, King's College London, Institute of Psychiatry, London SE5 8AF, UK
4 Department of Neurology, University of Cologne, 50924 Cologne, Germany
5 Department of Neurosurgery, University of Heidelberg, Heidelberg 60120, Germany
6 Imperial College London, London SW7 2AZ, UK
7 Department of Neurology, Charité Campus Mitte, 10117 Berlin, Germany
8 Centre for Stroke Research Berlin
9 Biomedical Engineering, University of Texas at Austin, TX 78712-0238, USA

*These authors contributed equally to this work.

Correspondence to: Prof Dr Rudolf Graf,
Max Planck Institute for Neurological Research,
Gleueler Str. 50,
50931 Cologne, Germany
E-mail: rudolf.graf@nf.mpg.de

How does infarction in victims of stroke and other types of acute brain injury expand to its definitive size in subsequent days? Spontaneous depolarizations that repeatedly spread across the cerebral cortex, sometimes at remarkably regular intervals, occur in patients with all types of injury. Here, we show experimentally with *in vivo* real-time imaging that similar, spontaneous depolarizations cycle repeatedly around ischaemic lesions in the cerebral cortex, and enlarge the lesion in step with each cycle. This behaviour results in regular periodicity of depolarization when monitored at a single point in the lesion periphery. We present evidence from clinical monitoring to suggest that depolarizations may cycle in the ischaemic human brain, perhaps explaining progressive growth of infarction. Despite their apparent detrimental role in infarct growth, we argue that cycling of depolarizations around lesions might also initiate upregulation of the neurobiological responses involved in repair and remodelling.

Introduction

A group of recent studies have established that, among the factors that may affect evolution of acute brain injury in its broadest sense, there is a substantial incidence of spontaneous depolarization events that propagate across the cerebral cortex in patients who have required urgent craniotomy for traumatic brain injury (Strong *et al.*, 2005), for aneurysmal subarachnoid haemorrhage (Dreier *et al.*, 2006), for malignant hemispheric stroke (Dohmen *et al.*, 2008) or for intracerebral haematoma (Fabricius *et al.*, 2008). Such waves of cortical spreading depolarization (CSD) recently termed 'killer waves' (Iadecola, 2009) affect essentially all neurons and astrocytes in their path; they were originally described by Leão (1944*b*), who delivered a local, mild insult to the cortex to elicit the phenomenon. Leão measured CSD indirectly using extracellular recordings of (i) the associated negative direct current shift (Leão, 1947) and (ii) the 'spreading depression' of electrocorticographic activity (Leão, 1947). At the level of a single neuron, CSD is characterized by a depolarization to nearly zero membrane potential, which is achieved by the combination of a reduced electrochemical gradient for potassium and the opening of persistent sodium and potassium conductances (Somjen, 2004).

Work in many laboratories over the past three decades with experimental models of these four clinical conditions has repeatedly demonstrated that CSD arises spontaneously in the surroundings of freshly developing brain lesions, propagating typically at 2–3 mm/min. The term 'peri-infarct depolarization' (PID) (Mies *et al.*, 1993; Hossmann, 1996) describes these events, especially for focal experimental stroke, when it occurs in tissue that is functionally disturbed and has diminished vascular and metabolic reactivity, but is not yet irreversibly committed to necrosis ('penumbra'; Astrup *et al.*, 1981). Experimental findings suggest that further growth of infarct size is proportional to the number of PIDs (Mies *et al.*, 1993) or to their aggregate duration (Dijkhuizen *et al.*, 1999), and that PID number is the independent, determining variable in this relationship (Busch *et al.*, 1996). The basis for this relationship may lie in abnormal microvascular vasoconstriction in response to the depolarization (Dreier *et al.*, 1998; Shin *et al.*, 2006; Strong *et al.*, 2007), and/or in one or more severe challenges to metabolism such as depletion of the tissue glucose pool (Nedergaard and Astrup, 1986; Vespa *et al.*, 2003; Hopwood *et al.*, 2005; Hashemi *et al.*, 2009). The detrimental role of PIDs may be enhanced by the fact that they often emerge in clusters, each with striking periodicity (Dreier *et al.*, 2006; Dohmen *et al.*, 2008).

Critically, little detail is known of the spatial spread of these waves of depolarization in the periphery of lesions and thus the spatial aspect of the relation between PIDs and infarct growth. We used the perfusion response to depolarization, already described in the early work of Leão (1944*a*) and often investigated thereafter (Hansen *et al.*, 1980; Lauritzen *et al.*, 1982), as a surrogate tracker of depolarization that can now be mapped visually in real time using laser speckle flowmetry (LSF) (Dunn *et al.*, 2001) (see Supplementary material 'Note 1'). Direct current electrodes were also used to verify depolarization events.

Here, we describe (i) patterns of spatial spread of depolarizations for the whole circumference of an ischaemic focus in an existing stroke model—permanent occlusion of a distal branch of the middle cerebral artery (dMCAO) in rats. Unexpectedly, and of considerable interest, we observed in this model that PIDs rotated or cycled, often several times, around the small focus. In the light of these findings, we examined (ii) the spatial behaviour of PIDs after permanent occlusion of the middle cerebral artery (MCA) in cats in detail, here and in a previous dataset available to us from another laboratory (London) (Strong *et al.*, 2007). We assessed patterns of PID spread (as seen in the restricted fraction of the ischaemic territory that can be imaged in this model) for evidence of compatibility with the concept of peri-lesion cycling. We then (iii) document PID occurrence and corresponding circular lesion growth assessed by MRI in a human patient suffering from 'malignant' hemispheric MCA infarction (Hacke *et al.*, 1996) and finally (iv) compare periodicity in the occurrence of peri-lesion depolarizations in malignant stroke patients derived from another, previous data set (Dohmen *et al.*, 2008) with equivalent experimental results in rats and cats, prompted by the suggestion that inter-depolarization interval might increase as absolute lesion volume increases in the progression from rat, to cat, to human.

Materials and methods

Adult male rats and adult female cats were used (but see also Supplementary material 'Note 2'). The study was approved by the local Animal Care Committee and the Regierungspräsident of Köln and is in compliance with the German Laws for Animal Protection.

Anaesthesia and surgical preparation in animals

Rat experiments

In six adult Wistar rats weighing 340–714 g, general anaesthesia was induced with halothane (4%) and maintained with isoflurane (0.8–1.2%) in a 70% nitrous oxide/30% oxygen gas mixture. The left femoral artery and vein were cannulated for continuous measurement of mean arterial blood pressure and serial measurement of blood gases (arterial $p_{ti}O_2$, $p_{ti}CO_2$, pH), and for i.v. administration of fluid and drugs, respectively. After tracheotomy and immobilization with pancuronium bromide (0.1 mg/kg, i.v.), artificial ventilation was started; immobilization was maintained throughout the experiment by intravenous infusion of Ringer's solution containing gallamine triethiodide (5 mg/kg/h). Acid–base balance was controlled using sodium bicarbonate. Deep body temperature was maintained at 37°C using a heating blanket servo-controlled by a rectal temperature probe. In order to produce small cortical ischaemic lesions in the MCA territory, we used a tandem occlusion method: occlusion of a distal branch of the MCA was combined with occlusion of the ipsilateral common carotid artery (Ohta *et al.*, 1997). In brief, the common carotid artery was first ligated. A hemicraniectomy (1.5 × 1.0 cm) was then performed over the left hemisphere, the cortex exposed and protected with warm mineral oil and imaging then started using LSF (see below). After acquiring control images, the frontoparietal branch of cortical MCA was coagulated and cerebral blood flow change was monitored for 6 h.

Cat experiments

For full details please see Supplementary material 'Note 2'.

In a total of seven cats (Cologne) and nine cats (London), anaesthesia was induced with ketamine or medetomidine/halothane (London) and maintenance anaesthesia was established with halothane (0.6–1.2%) in a 70% nitrous oxide/30% oxygen gas mixture. The left femoral artery and vein were cannulated for continuous measurement of mean arterial blood pressure and serial measurement of blood gases (arterial $p_{ti}O_2$, $p_{ti}CO_2$, pH), and for i.v. administration of fluid and drugs, respectively. Ringer's solution containing gallamine triethiodide (5 mg/kg/h) was infused intravenously (3 ml/h) for immobilization throughout the experiment. Acid–base balance was controlled using sodium bicarbonate. The right MCA was exposed transorbitally to be later occluded using either a device for remote occlusion or a clip (London). Deep body temperature was maintained at 37°C using a heating blanket servo-controlled by a rectal temperature probe. A mineral oil pool was established above the exposed cortex, its temperature servo-controlled to around 37°C and imaged as in experiments in rats. For maintenance of anaesthesia throughout the experiment, continuous α-chloralose infusion (5 mg/kg/h) was started following an initial bolus (60 mg/kg/15 min, i.v.).

Speckle image instrumentation and acquisition

The LSF method was implemented as previously described (Dunn *et al.*, 2001; Strong *et al.*, 2006). In brief, the cortex was illuminated with a laser diode (Sanyo DL7140-201, 785 nm, 70 mW, SANYO Electric, Tokyo, Japan) via a diverging lens and scattered light was assessed by a CCD camera (CT150A, CTec Photonics, Modesto, CA, USA). With our custom written software implemented on a 3.2 GHz Xeon processor, the inverse of the laser speckle contrast (inverse correlation time) was calculated for each pixel and the value was used for cerebral blood flow assessment in the next step. Since laser speckle contrast is inversely proportional to perfusion over the range of levels of perfusion tested, the inversion of the speckle image is linearly related to perfusion and we used the equation, cerebral blood flow (ml/100 g/min) = (inverse correlation time − 650)/273 to calculate 'indicative' values of perfusion (Strong *et al.*, 2006). Since the relationship of LSF with perfusion is not sufficiently robust to allow formal calibration, the values for cerebral blood flow reported here in units of ml/100g/min should be regarded as 'indicative' rather than 'absolute', and we therefore use the designation 'CBF$_{IND}$' (indicative cerebral blood flow) to reflect this qualification. However, they do allow good estimation of the true magnitude of cerebral blood flow changes. The highest rate of image acquisition was 12 images/min and it enabled us to see the cerebral blood flow dynamics in the cranial window.

Region of interest analysis of indicative cerebral blood flow

To assess regional CBF$_{IND}$ changes (e.g. to verify ischaemic changes before and after MCA occlusion, or perfusion changes on the propagation path of a CSD wave), small circular regions of interest (diameter as indicated in figure legends) were positioned avoiding larger vessels or bubbles in the mineral oil pool and CBF$_{IND}$ was calculated with our custom written software (VINCI: http://www.mpifnf.de/vinci/).

The change in CBF$_{IND}$ between pre- and post-MCA occlusion was analysed in each individual. The number of regions of interest that were set on the field was seven in rat and nine in cat cortex. The value at one time point was averaged from 10 consecutive images. As a measure of degree of ischaemia in each region of interest, the ratio of post- to pre-MCA occlusion cerebral blood flow was calculated.

To analyse CSD propagation, we used the CBF$_{IND}$ wave as surrogate for CSD propagation and the following criteria were applied for the designation of an event as a depolarization wave in the cat MCA occlusion experiments: (i) CBF$_{IND}$ change, either increase or decrease, should be not less than 10 ml/100 g/min; and (ii) propagation velocity should be less than 7 mm/min. We set this criterion higher than 3 mm/min, the propagation velocity that has typically been quoted for CSD, because higher values have been reported in brain slices (Aitken *et al.*, 1998).

Electrocorticography recordings in patients

First, we report on results derived from a patient who suffered from a large infarction of the MCA territory. After a decision had been made that, independent of the study, surgery was required for decompressive hemicraniectomy, we placed a subdural electrocorticography (ECoG) strip electrode containing six individual electrodes on the peri-infarct tissue of the cortex accessible from the craniectomy. Bipolar recordings were obtained from neighbouring electrodes (as described above) so that four ECoG channels were obtained; one electrode served as ground (Dohmen *et al.*, 2008). The patient was ventilated and sedated (fentanyl plus midazolam) throughout the monitoring. Simple visual detection of spreading depolarizations and periods of ECoG depression during the online measurement was achieved by displaying the high-pass filtered ECoG signal (lower frequency limit 0.5 Hz) and the power of the high-pass filtered ECoG signal (Fabricius *et al.*, 2006). The duration of ECoG depression until recovery (interval between depression onset and onset of restoration of activity) (Dreier *et al.*, 2006) was measured as an indirect indicator of the tissue energy status, since restoration of ECoG activity after spreading depolarization is energy dependent.

We performed a new analysis of the raw ECoG data of the patients included in a former study on malignant hemispheric stroke (Dohmen *et al.*, 2008), focusing now on timing of spreading depolarization events. To detect evidence for cycling (implying repeated transit of depolarization events across/along the electrode strip in one direction only), we considered for inclusion only events recurring (≥2) and spreading in one direction between the four channels (bipolar montage) on the subdural electrode strip. Original recordings from eight patients were available for this analysis. A total of 947.6 h of ECoG monitoring (mean duration of monitoring was 118.5 h ± 32.3 h) was scanned for spreading depolarizations fulfilling the above criteria. On these criteria we identified 97 intervals in seven patients. Eighty-seven of these 97 intervals (90%) showed a duration of <150 min and are displayed with this time axis in Fig. 6 for better interspecies comparison. Of 97, 10 intervals (10%) lasted >150 min.

Magnetic resonance imaging in patients

MRI was performed on a 1.5 T whole-body scanner (Philips Intera Master, Philips, Eindhoven, The Netherlands) in an axial direction (20 slices, 6 mm slice thickness, 0.6 mm interslice gap, field of view 23 cm, repetition time 3875 ms, echo time 95 ms, echo planar imaging 77).

Statistical methods

Values of continuous variables are given as mean ± standard deviation unless otherwise stated. In the rat dMCAO model, the difference in regional CBF_{IND} between pre- and post-dMCAO was tested with the Wilcoxon rank sum test. In the cat proximal MCA occlusion model of stroke, inspection of the CBF_{IND} maps as they evolved after MCA occlusion typically showed the emergence of a clear demarcation between a core area of very low perfusion, and adjacent cortex with better but not normal perfusion. Static perfusion values here were not formally analysed, since such analysis would serve only to replicate previously published work (Strong *et al.*, 2007). Instead, we analysed the spatial behaviour of transient, spreading changes in perfusion in the peri-infarct region.

Results

Please view the online Supplementary Videos 1–3 in close conjunction with this text. Legends to the videos are available at the end of the Supplementary material.

Systemic variables

Measurements of systemic variables did not show any significant alterations between control and ischaemic conditions, determined systematically 3 h after dMCAO in rats and MCA occlusion in cats (Supplementary Table 1).

Peri-infarct depolarizations cycle around ischaemic foci in the rat cerebral cortex following distal middle cerebral artery occlusion

In order to image the spread of PIDs around the complete circumference of an occlusive ischaemic lesion, we performed a large craniotomy above the left cerebral cortex and occluded a distal branch of the MCA in rats (Fig. 1A): this approach proved suitable, although imaging was interrupted during performance of the occlusion. We used a tandem occlusion model with ligation of the ipsilateral common carotid artery and coagulation of the fronto-parietal branch of the MCA (Brint *et al.*, 1988). PIDs were verified with microelectrodes as intra-cortical direct current shifts. Concomitantly, LSF detected waves of regional blood flow ('CBF_{IND}', indicative of absolute values of cerebral blood flow: please see 'Materials and methods' section) alteration coupled to the depolarizations. These CBF_{IND} waves (surrogates for PID) allowed us to study propagation patterns of these alterations. Static analysis of circular regions of interest (diameter 2.0 mm, seven regions of interest per animal) placed on CBF_{IND} images adjacent to and further from the coagulation point, revealed that CBF_{IND} significantly decreased in both the two time points, namely immediately and 1 h after occlusion, compared with pre-ischaemic controls to 50% (*P* = 0.036, Wilcoxon rank sum) in three regions of interest near to—and to 80% (non significant) in four regions of interest more distant from—this point. The effect of dMCAO is shown in Fig. 1B; here, a CBF_{IND} threshold <15 ml/100 g/min was applied, demarcating the ischaemic zone in blue. A total of 35 CBF_{IND} waves were observed in six individual rats. These waves originated in 29/35 cases in the border zone of the ischaemic focus. In 6/35 cases (in two individuals), waves invaded the field of view from outside it, so that an origin could not be identified. We suspect that microfocal trauma, in particular at the border of the craniotomy, may have given rise to these depolarization events. Interestingly, all waves propagated circumferentially along the border of the ischaemic focus, including those arising outside the image field. They either cycled around the focus, often multiple times (Fig. 1C and Supplementary Video 1) or they split at the point of origin and travelled then as two waves around either side of the focus until they met at the opposite side and annihilated each other (Fig. 2).

Multiple CBF_{IND} waves, appearing often with regular periodicity in temporal clusters, were associated with a decrease in basal (inter-event) CBF_{IND} (analysed in a circular region of interest in the border zone of the primary infarct; Fig. 1D, left) and this decrease appeared to occur stepwise with consecutive events. All animals developing such clusters of depolarization events showed comparable decreases of inter-event CBF_{IND} (Fig. 1E, left). Similarly, the number of pixels below a CBF_{IND} threshold value <15 ml/100 g/min increased stepwise in the same circular region of interest (Fig. 1D and E, right) documenting the growth of the ischaemic focus in response to the number of depolarization events. In the example in Fig. 1, CBF_{IND} waves were characterized principally by hyperaemia. Detailed analysis of all 35 events in rat dMCAO revealed, however, that 17 waves were hyperaemic, 12 were biphasic with a hypoperfusion onset followed by a hyperaemic tail that was usually longer in duration and six waves consisted of monophasic hypoperfusion. In individual cases, dispersal of CBF_{IND} waves was wide enough to allow us to position small regions of interest in both inner and outer zones of the propagation path. In such cases, examination in inner zones near the ischaemic core showed biphasic hypo-/hyperaemic or monophasic hypoperfusion CBF_{IND} responses (that were sometimes sustained), whereas analysis of regions of interest in the outer zones always revealed monophasic hyperaemic responses (Fig. 2). Thus, depolarization-coupled CBF_{IND} responses in rat dMCAO are compatible with a gradient of perfusion developing in border zones of ischaemic foci after arterial occlusion, as described originally, to our knowledge, by Symon *et al.* (1974). Depolarizations also reduce perfusion further in the border zones, as has recently been described for MCA occlusion in mice (Shin *et al.*, 2006) and in cats (Strong *et al.*, 2007) using LSF real-time imaging.

Spatial patterns of spread of peri-infarct depolarizations in the gyrencephalic brain of the cat following proximal middle cerebral artery occlusion

In the light of the above findings, we next examined patterns of spread of PIDs around larger, occlusive ischaemic foci in the gyrencephalic brain. For this, we retrospectively reviewed spatial patterns of CBF_{IND} wave propagation in two sets of data (one set from the laboratory of A.J.S. in London and a second from this laboratory in Cologne) on MCA occlusion in the gyrencephalic
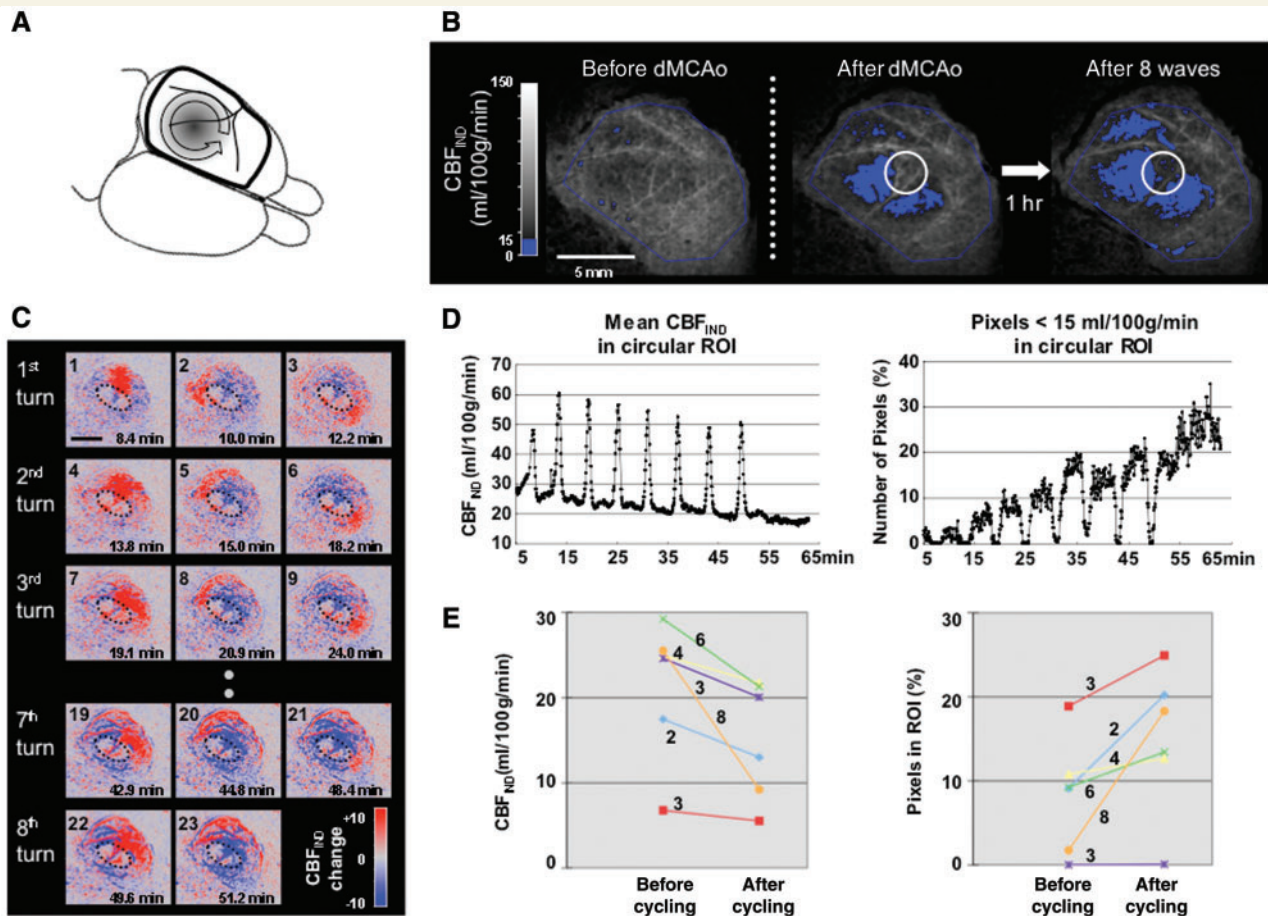
Figure 1 Repetitive cyclic CBF$_{IND}$ wave propagation around primary ischaemic lesion in rat cortex after dMCAO (see also Supplementary Video 1). (**A**) Diagram of the dorsal aspect of the rat brain. Frame (thick lines) indicates field of view for LSF. Vascular territory of distal MCA, ischaemic territory and anti-clockwise cycling (arrow) are indicated. (**B**) Expansion of the ischaemic lesion after repetitive propagation of eight cyclic CBF$_{IND}$ waves. A region of interest (white circle; 3 mm diameter) located in the boundary zone served for time course analysis of CBF$_{IND}$ and increase of number of pixels with CBF$_{IND}$ <15 ml/100 g/min (Fig. 2C and D). (**C**) Sequential images demonstrating multiple consecutive turns of CBF$_{IND}$ waves around the ischaemic lesion demarcated by dotted black line. Time after dMCAO is indicated in individual images. Please note that the surrounding of the ischaemic core turned progressively blue compared with the first image, indicating gradual expansion of the ischaemic core. (**D**) Time course of mean CBF$_{IND}$ (left) and number of pixels with CBF$_{IND}$ <15 ml/100 g/min (right) analysed in boundary zone region of interest (ROI) (Fig. 2B). CBF$_{IND}$ flow increased repetitively while basic CBF$_{IND}$ decreased stepwise during CBF$_{IND}$ wave passage. On the other side, the number of pixels with CBF$_{IND}$ <15 ml/100 g/min increased in the region of interest stepwise with CBF$_{IND}$ waves. (**E**) Decrease of basic CBF$_{IND}$ (left) and increase of the number of pixels with CBF$_{IND}$ <15 ml/100 g/min (right) in relation to number of CBF$_{IND}$ waves (numbers next to lines). Data analysed in the various rats using region of interest analysis as shown in Fig. 2D.

brain of cats (Strong *et al.*, 2007). The anatomical disposition of the ectosylvian, suprasylvian and marginal gyri, each set circumferentially and at respectively increasing distances from the Sylvian fissure and location of core ischaemia after proximal MCA occlusion, facilitates spatial and temporal analysis of spread of depolarizations (Figs 3 and 4). These figures also illustrate the restricted fraction of the ischaemic territory that we are able to image in cats undergoing MCA occlusion. Changes in perfusion in response to depolarization in these two groups of experiments have been reported previously, with the conclusion that the responses of perfusion to depolarization in the penumbra deteriorate progressively with increasing proximity to the core: monophasic hyperaemia on the medial marginal gyrus nearest collateral perfusion from the anterior cerebral artery, biphasic alteration (hypoperfusion then

hyperaemia) nearer, and monophasic hypoperfusion of varying durations, sometimes very sustained, immediately adjacent to the core (Strong *et al.*, 2007). The new analyses of spatial patterns of spread are described in detail in the Supplementary material 'Note 2' and the findings are summarized here. In aggregate, 142 events were analysed (60 in 9 London experiments all sampled continuously for 4 h after occlusion and 82 in 7 Cologne experiments followed for between 10 and 26.5 h after occlusion). Patterns of spread were in principle either radial (outwards from the core focus: 41% Cologne, 11% London) (Fig. 3 and Supplementary Video 2), or circumferential (spreading along the edge of the core: 59% Cologne, 89% London) along the length of one or more of the three exposed gyri, and circumferential PIDs often appeared in clusters with rather regular periodicity (Fig. 4 and
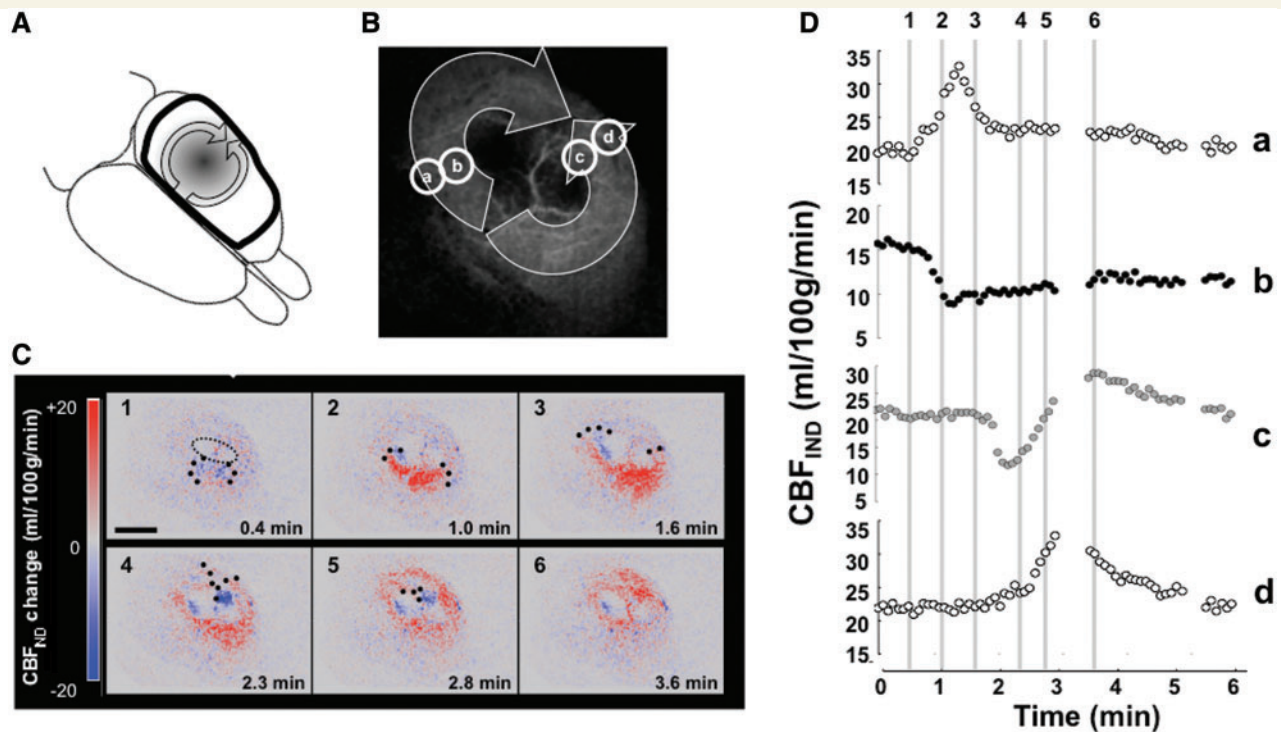
Figure 2 'Split' CBF_{IND} wave propagation around ischaemic lesion after rat dMCAO. (**A**) Diagram of the dorsal aspect of the rat brain indicates 'split' clockwise and anti-clockwise circumferential propagation of two CBF_{IND} waves (arrows) around the ischaemic lesion. (**B**) Laser speckle image shows darkened inner zone with ischaemic transition and schematic representation of propagating 'split' CBF_{IND} wave as well as positions of regions of interest in outer (a, d) and inner border zone (b, c) used for time course analysis of CBF_{IND}. (**C**) Sequential images demonstrating 'split' CBF_{IND} wave propagation around the ischaemic lesion (thin dotted black line in the first image). CBF_{IND} wave originated from one point in the ischaemic boundary zone, separated immediately into two waves, which then propagated in both directions around the ischaemic lesion to collide and vanish at the opposite side. Time after start of CBF_{IND} wave and propagation of the wave front (thick dots) is indicated in individual images. Black bar = 5 mm. (**D**) Time course of CBF_{IND} (left) in four regions of interest demonstrating in inner zones near the ischaemic core monophasic sustained hypoperfusion (region of interest b) or biphasic hypo-/hyperaemic response (region of interest c), whereas in outer zones always revealed monophasic hyperaemic responses were dominant (regions of interest a, d).

Supplementary Video 3). Five events in the London experiments that originated within the imaging field later in the observation period exhibited both radial and circumferential spread. In both laboratories, it seemed that events spreading radially most often occurred early in the course of post-MCA occlusion observation, whereas circumferential spread was seen later; however, this could not be verified formally and the basis for distinction between these two patterns of spread is considered in the 'Discussion' section. In the Cologne data, the initial core lesion was typically slightly smaller (most probably due to higher blood pressure and consequently better collateral perfusion), and this probably accounts for the higher incidence of radial spread than in London; with radial spread, a delay was invariably seen as the wave descended from suprasylvian gyrus into the marginal sulcus, before re-emerging onto the marginal gyrus (Fig. 3 and Supplementary Video 2).

The occasionally observed occurrence of circumferentially spreading events, either 'splitting' from a focus at the edge of the core, or entering the imaged field almost simultaneously from opposite sides as two events and propagating towards each other before colliding, is compatible with the hypothesis that PIDs in the gyrencephalic brain are capable of tracking around at least a major portion of the circumference of a focus of core ischaemia, as imaged around the entire core lesion in our rat dMCAO preparation. Whether PIDs originate at the edge of the core, or at new foci in the penumbra has been debated (Nedergaard and Hansen, 1993): the present data document origin at the edge of the core, but (temporally sporadic) circumferential events entering the field from outside may have arisen from either potential source. Given the visualization of a split of depolarization in rat dMCAO (Fig. 2), it is reasonable to suggest that dual events appearing (near)-simultaneously on the same gyrus (cat MCA occlusion) from opposite sides of the image field may reflect the same bifid pattern of origin and spread.

Peri-infarct depolarizations are associated with circular secondary growth of lesion in patients with large middle cerebral artery infarction

Clustering of depolarizations has now been also described in recent studies in patients with subarachnoid haemorrhage (Dreier et al., 2006) and ischaemic stroke (Dohmen et al., 2008) and
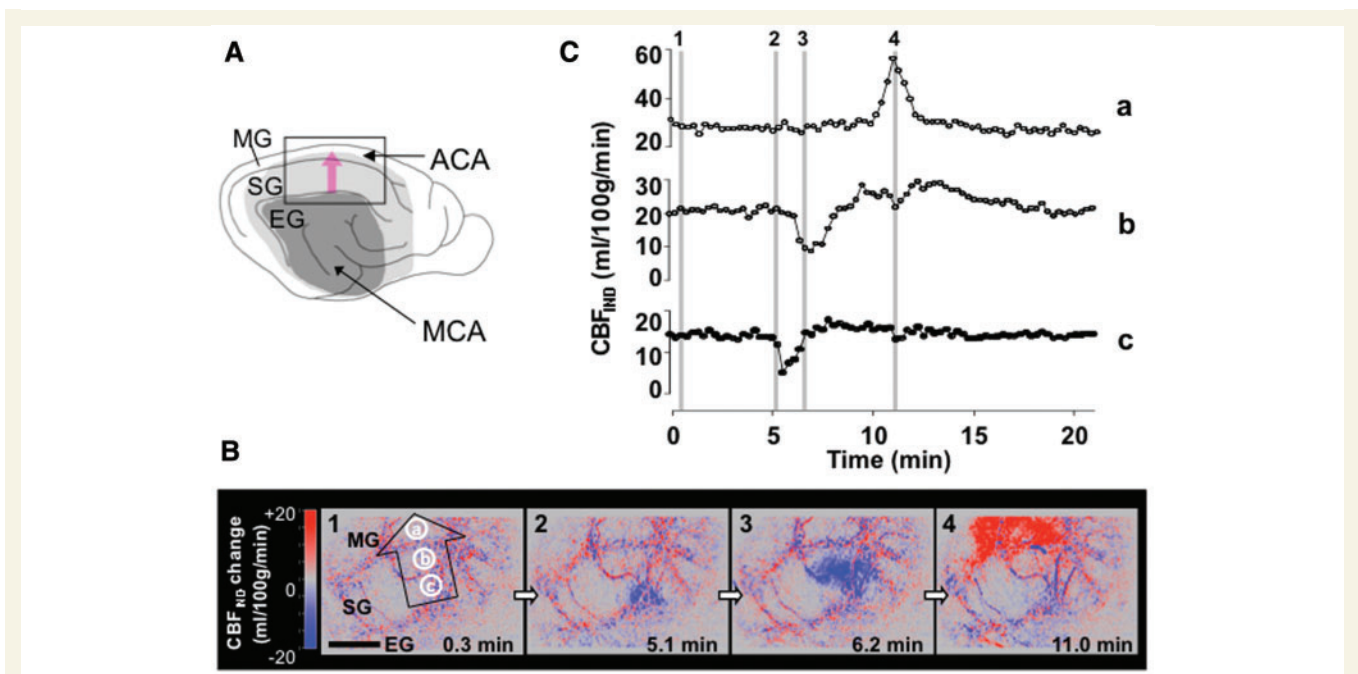
Figure 3 Radial CBF$_{IND}$ wave propagation in the ischaemic boundary zone after cat MCA occlusion (see also Supplementary Video 2). (**A**) Diagram of the lateral aspect of the cat brain with schematic representation of ischaemic core (dark grey) and border zone (light grey) after MCA occlusion. Arrows indicate territories of MCA and anterior cerebral artery (ACA), pink arrow indicates radial direction of CBF$_{IND}$ wave propagation. (**B**) Sequential images (1–4) of radial CBF$_{IND}$ wave propagating from inner ischaemic boundary zone (suprasylvian gyrus; SG) to periphery (marginal gyrus; MG). Colour coded CBF$_{IND}$ change indicates hypoperfusion appearance in the suprasylvian gyrus near the ischaemic core in blue, hyperaemic appearance in the MG in red as the wave travels into the ischaemic periphery. Time in images indicates time from onset of CBF$_{IND}$ wave and corresponds to time scale in Fig. 4C. Regions of interest a, b, c in first image served for time course analysis (Fig. 4C). (**C**) Time course of CBF$_{IND}$ in regions of interest a, b and c, showing the transition from hypo- to hyperaemic appearance as the wave propagates from inner to outer boundary zone of the ischaemic focus. EG = ectosylvian gyrus.

prompted a comparison of human and animal data with respect to circumferential propagation. We report here on new results in a patient suffering from malignant hemispheric MCA occlusion (Fig. 5). In this patient, PIDs were recorded using an electrode strip comprising six electrodes that was positioned subdurally over peri-infarct tissue, parallel to the infarct rim. This procedure was carried out at the conclusion of hemicraniectomy performed in order to decompress massive ischaemic oedema and brain swelling. From the six electrodes of the strip, four ECoG channels (A–D) were acquired. The ECoG depression and its duration are best visualized as a reduction of the power of the high-pass filtered ECoG amplitude, which also allows simple visual detection of PID during the online measurement at the bedside. Figure 5A shows PID measurements from a 53-year-old patient, who underwent hemicraniectomy 22 h after a large MCA infarction. Monitoring was started 29 h after stroke. During the first 24 h of monitoring, PIDs were detected only in channels D and C, spreading from D to C. Both channels were acquired from the electrodes located more proximal to the infarct rim. At later time points, PIDs progressively expanded spatially along the electrode strip involving channel B and finally also channel A (Fig. 5A), the channels from electrodes positioned further from the infarct. This expansion of depolarizing events along the strip electrode over time was accompanied by a progressive decline of the ECoG, which was more pronounced in channel D, resulting finally in an almost flat signal. Additionally, we observed an increasingly prolonged

duration of ECoG depression and recovery after each PID over time (Fig. 5A and B), again more pronounced in channel D than in channel A. Furthermore, repetitive PIDs occurred in this patient, often in clusters with regular periodicity (Fig. 5C), showing unidirectional propagation of multiple PIDs along the electrode strip, and therefore along the infarct rim. From the 92 depolarizations detected in this patient, 72 spread from channel D towards channel A (clockwise along the strip electrode and with regard to the edge of infarction) and 19 spread contrariwise towards channel D (counter clockwise along the strip electrode). In this same patient, we performed MRI for the first time both shortly after start (43 h, second day post-stroke) and at the end of ECoG monitoring (186 h, seventh day post-stroke), thus enabling us directly to assess alterations in infarct size occurring exactly during the period of ECoG monitoring (Fig. 5D). The follow-up MRI at Day 7, after 92 PIDs, showed substantial infarct growth, with recruitment of new cortical regions in comparison with the first MRI. Infarct growth and newly established lesions were best documented by diffusion-weighted imaging (Fig. 5D). In the surface reconstruction in particular, the concentric nature of this growth became evident. The mapping of apparent diffusion coefficients showed a reduction (hypointensity) of apparent diffusion coefficient precisely in the areas undergoing secondary ischaemia during the period of ECoG monitoring, indicating that delayed ischaemic transformation occurs in regions of secondary damage during the time of multiple PID passage.
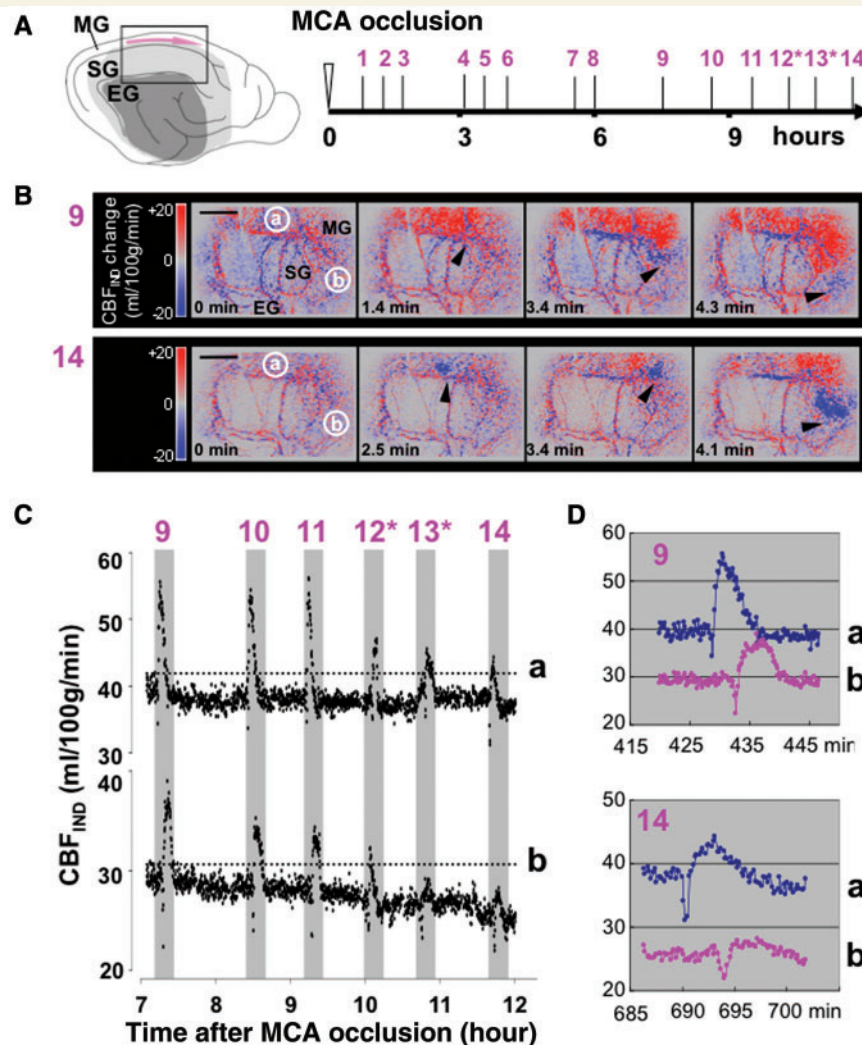
Figure 4 Circumferential CBF_{IND} wave propagation in the ischaemic boundary zone after cat MCA occlusion (see also Supplementary Video 3). (**A**) Diagram of the lateral aspect of the cat brain (see also Fig. 3A). Pink arrow indicates circumferential direction of CBF_{IND} wave propagation. Temporal emergence of 14 consecutive CBF_{IND} waves is indicated on the right. All waves (other than 12 and 13, asterisks) travelled clockwise. (**B**) Sequential images of waves 9 and 14 propagating circumferentially in marginal gyrus (MG) around the ischaemic focus. Time on images indicates time from onset of respective CBF_{IND} waves. Regions of interest a (on marginal gyrus; far from ischaemic core), b [on suprasylvian gyrus (SG); close to core] in first images served for time course analysis. Black bars = 5 mm. Arrow heads indicate wave front. Note that the wave front turns into hypoperfusion (blue) in 14th wave. (**C**) Time course of CBF_{IND} in regions of interest a and b showing consecutive waves 9–14. Waves 12 and 13 travelled anti-clockwise. The transition from hypo- to hyperaemic appearance as the wave propagates from inner to outer boundary zone of the ischaemic focus. Note the continuous decrease of baseline CBF_{IND} in the zone close to the ischaemic core (region of interest b). (**D**) Zoomed view of time course of CBF_{IND} waves 9 and 14, showing transition from biphasic (hypo- then hyperaemic) CBF_{IND} pattern in wave 9 to more pronounced hypoperfusion pattern in wave 14, particularly in region of interest b. EG = ectosylvian gyrus.

Inter-species comparison of depolarization frequencies

In the light of the above findings we analysed and compared retrospectively the intervals between (i) unidirectionally propagating CSDs in seven patients with hemispheric stroke experiencing clusters of depolarizations (Dohmen *et al.*, 2008); (ii) unidirectionally propagating CBF_{IND} waves in seven MCA occlusion experiments in cats; and (iii) cycling CBF_{IND} waves in the dMCAO model in six rats. The resulting inter-event interval histograms (Fig. 6) demonstrate that in rat dMCAO, the modal interval is

considerably shorter than in cat proximal MCA occlusion, consistent with a smaller absolute lesion volume (see Supplementary material 'Note 3'). Although intervals between consecutive depolarization events in CSD/PID clusters in human malignant stroke were rather longer than in the cat, any difference is less marked than between cat and rat, and this is addressed in the 'Discussion' section. This finding suggests that periodicity of occurrence at relatively regular intervals is not only a common feature of PIDs but that periodicity may result at least in many instances from circumferential multiple propagation of depolarizations around ischaemic core lesions.
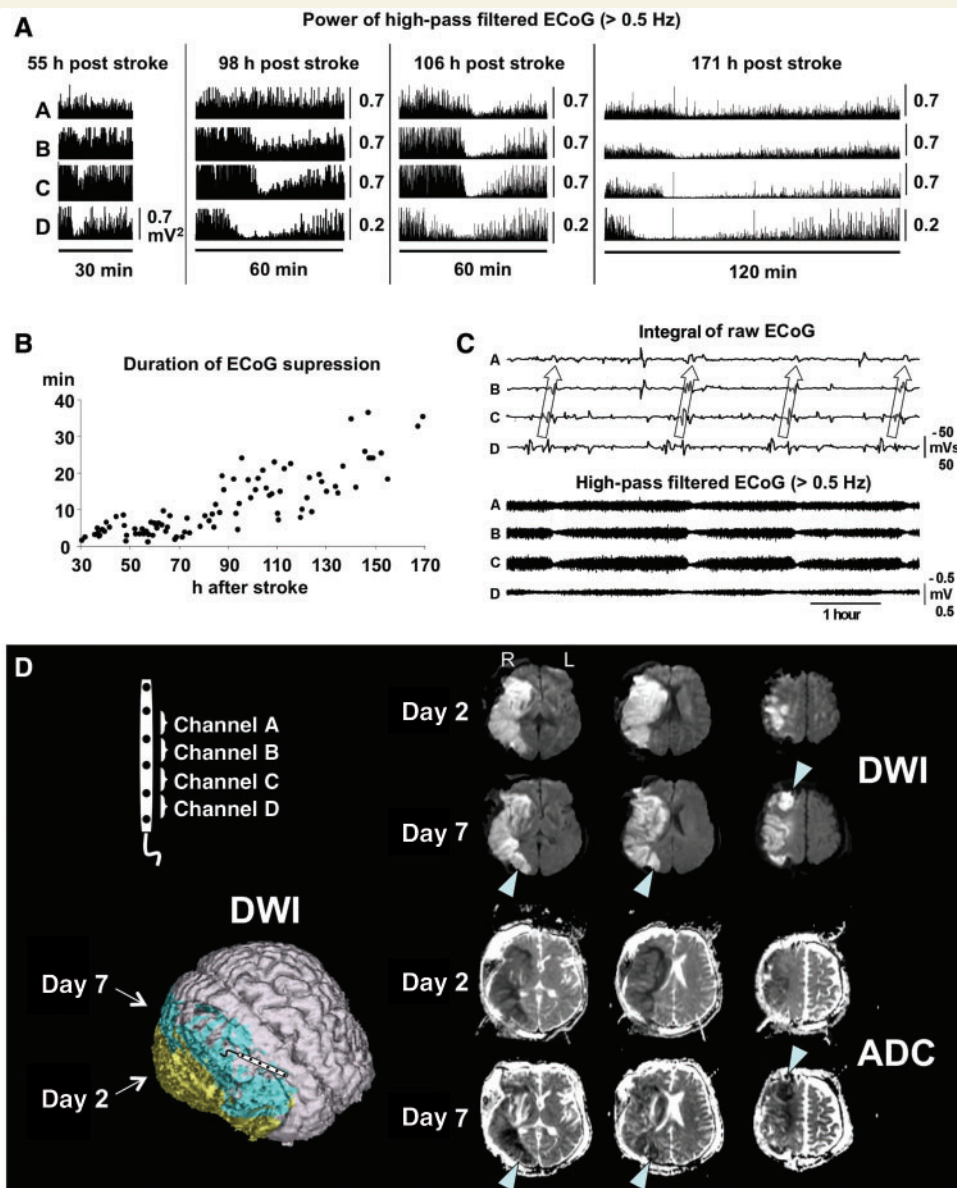
Figure 5 Secondary infarct growth related to multiple appearance of CSD in a patient suffering from 'malignant' ischaemic stroke. (**A**) From the six electrodes of the subdurally implanted electrode strip, ECoG channels A, B, C and D were acquired. CSD associated ECoG depression expanded spatially along the strip electrode from channel D and C to B and finally also A over time. The ECoG signal progressively decreased with repeated CSDs (note the change of scale from 0.7 to 0.2 mV^2 in channel D after first episode). (**B**) In addition, the duration of ECoG suppression and ECoG recovery after each CSD was increasingly prolonged indicating a progressive metabolic deterioration in underlying tissue. (**C**) Repetitive unidirectional propagations of CSDs at intervals with comparable duration in the ischaemic boundary zone (see arrows) appear as slow potential changes of the integrated raw ECoG (upper panel) and as successive reductions of the high-pass filtered ECoG (lower panel). Since each channel displays the potential difference between its two active electrodes, the spread of the slow potential change from one electrode to the next is seen from the phase reversal between two neighbouring channels sharing a common electrode. (**D**) MRI was conducted after start of monitoring on Day 2 and at the end of monitoring on Day 7 after stroke. The follow-up MRI showed a growth of infarction with secondary ischaemia of the peri-infarct tissue in which 92 CSDs had occurred over the course of around 5 days of monitoring. Note the newly established lesions around the primary infarct area in the diffusion weighted imaging (DWI) on Day 7 corresponding to reduced apparent diffusion coefficients (ADC) in the same regions (see arrow heads) indicating the process of secondary deterioration. The strip electrode (schematically displayed) was placed over peri-infarct tissue, tangentially to the infarct border, with electrodes generating channel D closest to and electrodes generating channel A most distant to the infarct. Note the concentric pattern of cortical infarct growth.
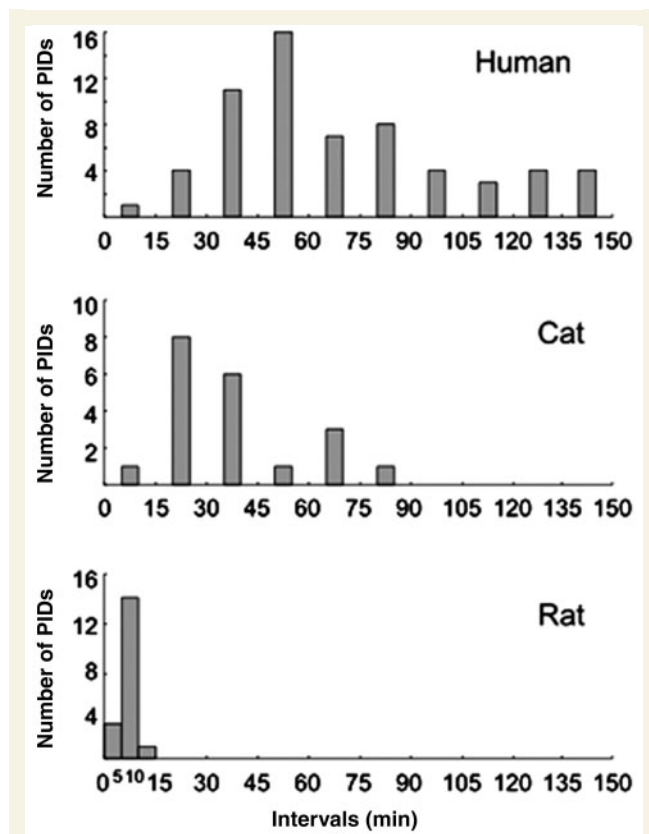
Figure 6 Inter-species comparison of CSD periodicity. Time interval histograms are shown between recurrent cyclic CBF_{IND} waves after dMCAO in rats ($n = 6$), circumferential CBF_{IND} waves after proximal MCA occlusion in cats ($n = 7$) and spreading depolarizations in human malignant hemispheric stroke appearing in clusters of CSD ($n = 7$). Please note that intervals propagating unidirectionally were analysed in cats and human patients. Distributions reveal (i) intervals to be shorter in rats than in cats and humans and (ii) that in humans, intervals are distributed more widely than in cats and rats.

Discussion

The principal finding in this study was the detection of a wave of cortical blood flow alteration secondary to a depolarization that cycled, spontaneously and several times, around a focal ischaemic lesion in the lissencephalic brain of rats. This gave rise to the observation, at any single given point in the wave path, of recurrent blood flow transients with quite regular periodicity—in temporal terms a 'cluster'—and the imaging data allowed not only interpretation of such clustering as indicating repetitive peri-lesion cycling of a single depolarization wave, but also demonstrated considerable stepwise enlargement of the ischaemic lesion with each single wave cycle. In the gyrencephalic brain of cats, we identified similar repetitive circumferential propagation around larger ischaemic lesions imaged, however only in a sector of perhaps some 75° of the full 360° of the evolving infarct. Furthermore, the observation that multiple, partially clustered, repetitive PIDs in a patient with malignant hemispheric stroke coincided with major, essentially concentric enlargement of the

ischaemic lesion over a period of 5 days led to the inference that the experimental results may apply at least to some extent to human stroke.

The present results demonstrate behaviour similar (in respect of cycling around an anatomical lesion) to that underlying a cardiac arrhythmia that is common in humans, atrial flutter (Murgatroyd and Krahn, 2002), and also indicate that repetitive peri-lesion cycling of a depolarization is a property of cerebral cortex undergoing a naturally occurring pathological process—occlusive ischaemia. Thus peri-lesion cycling does not require surgical lesioning of the cortex to impose a pathway of cyclical propagation, as first described by Shibata and Bures (1972), and is not confined to specially designed preparations of central nervous tissue such as the isolated chick retina (Martins-Ferreira et al., 1974). The findings in rat focal ischaemia accord well with—and offer an explanation for—periodicity in clusters of spreading depolarizations as observed in peri-infarct tissue in the gyrencephalic brain of cats (Ohta et al., 1997) and also in patients with acute ischaemic brain injury (Dreier et al., 2006; Dohmen et al., 2008).

It is remarkable that the circling pattern of PID propagation was consistently observed in rats despite the fact that the experiments in this species were carried out under isoflurane/nitric oxide anaesthesia. This type of anaesthesia is known to attenuate CSD susceptibility in non-ischaemic rat brain (Kudo et al., 2008). The penumbra seems to be more susceptible to CSD than non-ischaemic cortex, based on the observation that known inhibitors of CSD (e.g. NMDA receptor blockers) are less likely to inhibit PIDs in ischaemic penumbra (Shin et al., 2006) or when the cortex is conditioned by artificially elevated extracellular K^+ (Petzold et al., 2005). Our results indicate therefore that the probability for PID induction and propagation is very high in the penumbra, and might even be augmented under other anaesthetics like α-chloralose, or in the awake state.

After the very acute phase of ischaemic and metabolic failure and damage, lesion growth into the penumbra may persist for hours or even days (Heiss et al., 1994). Lesion growth 'pari passu' with occurrence of individual CSDs has been shown with nicotinamide adenine dinucleotide fluorescence imaging (Strong et al., 1996) and, now in a sequence of CSDs, with LSF (Shin et al., 2006). The present findings are important in showing that sequences of depolarizations can occur and serve to deepen and widen the ischaemia on the basis of repetitive cycling and coupled stepwise deterioration in perfusion around a focus of sustained depolarization in the cerebral cortex—the initial core lesion. [Occurrence of spreading depolarizations in deep grey nuclei is also well documented, both in the human (Sramka et al., 1977) and in the cat (with evidence suggesting temporal clustering) (Umegaki et al., 2005).]

Our review of spatial patterns of spread of depolarizations in the cat MCA occlusion model yielded data compatible with, and strongly suggestive of, cycling of depolarizations around the ischaemic core. Thus we saw examples of circumferential and radial spread, and of depolarizations that split from an origin at the edge of the core, to spread both clockwise and anti-clockwise around the core. Conversely, we recorded more than one instance where depolarizations emerged from either side of the field and collided, suggesting an origin from a single start point diametrically

opposite on the lesion perimeter. However, the limitations imposed by the restricted field of view in this model are significant; for example, dual, simultaneous converging events may alternatively have arisen from new, separate initiation sites at the rim of the core, both of them precipitated by a transient reduction in arterial pressure. Given the restricted fraction of the ischaemic territory that can be imaged in these experiments, greater reliance has to be placed on the demonstration of recurrent depolarizations at reasonably repetitive time intervals (perhaps within 10–15%) as evidence for cycling. That the incidence of tight periodicity is not as high in the cat MCA occlusion preparation as with rat dMCAO does not argue against this hypothesis; this is because the longer perimeter of the core in the cat brain raises the probability of additional, new depolarizations originating at the perimeter and interrupting regular repetition of a cycling wave.

Are we justified in applying the spatial cycling model to human ischaemic brain injury? The relatively tight periodicity of depolarizations shown in Fig. 5 from a patient with malignant hemispheric stroke supports this suggestion. However, although the increase in modal interval between clusters of depolarizations as we move from rat to cat brain appears appropriate in relation to the likely absolute lesion perimeter, this argument cannot be sustained when comparing intervals between events in cat versus human brain. A much longer modal interval would be expected of cycling around an MCA infarct in humans than is indicated in Fig. 6. The discrepancy may be explained in two ways (that are not mutually exclusive). First, the much longer (absolute) lesion perimeter in humans (MCA occlusion) increases the probability of new events arising on the perimeter, interrupting any regular cycling observed at the relatively localized site of a single recording strip on the lesion periphery. Second, where clear periodicity is seen with a modal interval of the order we describe, this would suggest the possibility of cycling around a smaller, evolving 'satellite' core situated within what is still largely penumbra. Such heterogeneity has been described, at least in experimental stroke models (Tomlinson *et al.*, 1993).

Critically, the demonstration of repetitive peri-lesion cycling of a depolarization introduces the novel hypothesis that this behaviour may not simply cause lesion growth but also serve as a biological amplifier, enhancing upregulation around a lesion of inflammatory, stress- and neurogenic-response cascades to focal brain injury that are known to be related to spreading depolarization (Sharp *et al.*, 2000; Jander *et al.*, 2001; Gursoy-Ozdemir *et al.*, 2004; Yanamoto *et al.*, 2005). This could potentially apply to any tissue in the central nervous system capable of supporting CSD, namely a concentration of neuronal cell bodies, astrocytes (or Müller cells in the retina) and their associated vasculature— whether in the cerebral cortex, deep nuclei (Sramka *et al.*, 1977), brainstem (Richter *et al.*, 2003), spinal cord (Czeh and Somjen, 1990) or retina. As an example of a pathogenic effect of CSDs, matrix-metalloproteinase-9 upregulation increases blood–brain barrier permeability (Gursoy-Ozdemir *et al.*, 2004) and hence can promote vasogenic oedema. On the positive side, deliberate preconditioning of the rat cerebral cortex with CSD confers a measure of protection against a subsequent ischaemic challenge (Kobayashi *et al.*, 1995). However, it is very clear now

that repetitive CSDs under conditions of focal ischaemia—PIDs— cause vasoconstriction in the microcirculation (Dreier *et al.*, 1998; Shin *et al.*, 2006; Strong *et al.*, 2007) and hence promote lesion expansion and/or deterioration towards terminal depolarization and infarction. The data in Fig. 1C (circumferential spread of depolarization: rat) and Supplementary Video 2 (nakamura_suppl _v2.mov) (radial spread: cat) suggest that the time course of the perfusion response to PID is biphasic nearest the core (hyperaemia followed by hypoperfusion in the rat: hypoperfusion followed by mild hyperaemia in the cat) but monophasic (hyperaemia: either species) more remotely and nearer sources of collateral perfusion. This is consistent with the observation of impaired neurovascular coupling at the infarct border (Kunz *et al.*, 2007), although the relative phasing of hyperaemia and hypoperfusion may vary between species (Strong *et al.*, 2007). The precise features of ischaemia that determine the apparently critical reversal of the vascular response to depolarization from dilation to constriction remain to be identified, but recent work suggests that downregulation of the endothelial nitric oxide synthase pathway contributes to this reversal (Petzold *et al.*, 2008).

The present results do not by themselves prove that PIDs are pathogenic in the human brain, in terms of specific histological or structural MRI findings that can be related to number and/or patterns of depolarizations. A prospective study of this nature is desirable. However, three elegant experimental studies suggest that number of PIDs is an independent predictor of infarct size (Back *et al.*, 1996; Busch *et al.*, 1996; Takano *et al.*, 1996). In addition, new clinical monitoring data indicate that some depolarizations may be accompanied by reductions in cerebral blood flow suggesting vasoconstriction (Dreier *et al.*, 2009), and often by depletion of the interstitial brain glucose pool (Feuerstein *et al.*, 2010), suggesting a pathogenic potential.

These features, especially when set against the suggestion (above) that CSD associated with the (more normal) hyperaemic response may be protective, raise the issue of clinical management. Briefly, we submit that clearer evidence of the relationships of different patterns of depolarizations—dilator or constrictor— with outcome is needed before specific therapy can be designed. Clinical application would probably be dependent first on distinction of these two patterns in individual patients, and should recognize (i) that blockade of hyperaemic (normal response) CSD may compromise a response that is potentially protective and (ii) that PIDs are unlikely to respond to glutamate antagonists (Shin *et al.*, 2006) [although earlier experimental work with a gyrencephalic MCA occlusion stroke model suggested that post-treatment with MK801 is protective (Park *et al.*, 1988), and there is initial clinical evidence to suggest that it may sometimes be possible to block depolarizations (Sakowitz *et al.*, 2009)]. Until it is clear which patterns of depolarization are independently associated with better or worse outcome, medical management should probably focus simply on careful application of some principles of good clinical management: avoidance of hypotension and pyrexia (Hartings *et al.*, 2009) and maintenance of an adequate but not excessive plasma glucose, most probably in the range 7–9 mmol/l (125–160 mg/100 ml) (Oddo *et al.*, 2008; Strong, 2008).

In conclusion, the present findings explain observations of periodicity in CSD occurrence in acute brain injury and the impact of

CSDs on infarct size. Future work should address what determines (i) variation between adverse and restorative-protective responses and (ii) clinical outcome in human brain injury, and only then should focus on the central goal of effective therapy.

Acknowledgements

Funding

Supplementary material

Supplementary material is available at *Brain* online.

References

Aitken PG, Tombaugh GC, Turner DA, Somjen GG. Similar propagation of SD and hypoxic SD-like depolarization in rat hippocampus recorded optically and electrically. J Neurophysiol 1998; 80: 1514–21.

Astrup J, Siesjo BK, Symon L. Thresholds in cerebral ischemia - the ischemic penumbra. Stroke 1981; 12: 723–5.

Back T, Ginsberg MD, Dietrich WD, Watson BD. Induction of spreading depression in the ischemic hemisphere following experimental middle cerebral artery occlusion: effect on infarct morphology. J Cereb Blood Flow Metab 1996; 16: 202–13.

Brint S, Jacewicz M, Kiessling M, Tanabe J, Pulsinelli W. Focal brain ischemia in the rat: methods for reproducible neocortical infarction using tandem occlusion of the distal middle cerebral and ipsilateral common carotid arteries. J Cereb Blood Flow Metab 1988; 8: 474–85.

Busch E, Gyngell ML, Eis M, Hoehn-Berlage M, Hossmann KA. Potassium-induced cortical spreading depressions during focal cerebral ischemia in rats: contribution to lesion growth assessed by diffusion-weighted NMR and biochemical imaging. J Cereb Blood Flow Metab 1996; 16: 1090–9.

Czeh G, Somjen GG. Hypoxic failure of synaptic transmission in the isolated spinal cord, and the effects of divalent cations. Brain Res 1990; 527: 224–33.

Dijkhuizen RM, Beekwilder JP, van der Worp HB, Berkelbach van der Sprenkel JW, Tulleken KA, Nicolay K. Correlation between tissue depolarizations and damage in focal ischemic rat brain. Brain Res 1999; 840: 194–205.

Dohmen C, Sakowitz OW, Fabricius M, Bosche B, Reithmeier T, Ernestus RI, et al. Spreading depolarizations occur in human ischemic stroke with high incidence. Ann Neurol 2008; 63: 720–8.

Dreier JP, Major S, Manning A, Woitzik J, Drenckhahn C, Steinbrink J, et al. Cortical spreading ischaemia is a novel process involved in ischaemic damage in patients with aneurysmal subarachnoid haemorrhage. Brain 2009; 132: 1866–81.

Dreier JP, Korner K, Ebert N, Gorner A, Rubin I, Back T, et al. Nitric oxide scavenging by hemoglobin or nitric oxide synthase inhibition by N-nitro-L-arginine induces cortical spreading ischemia when K+ is increased in the subarachnoid space. J Cereb Blood Flow Metab 1998; 18: 978–90.

Dreier JP, Woitzik J, Fabricius M, Bhatia R, Major S, Drenckhahn C, et al. Delayed ischaemic neurological deficits after subarachnoid haemorrhage are associated with clusters of spreading depolarizations. Brain 2006; 129: 3224–37.

Dunn AK, Bolay H, Moskowitz MA, Boas DA. Dynamic imaging of cerebral blood flow using laser speckle. J Cereb Blood Flow Metab 2001; 21: 195–201.

Fabricius M, Fuhr S, Bhatia R, Boutelle M, Hashemi P, Strong AJ, et al. Cortical spreading depression and peri-infarct depolarization in acutely injured human cerebral cortex. Brain 2006; 129: 778–90.

Fabricius M, Manning A, Hartings JA, Sakowitz OW, Woitzik J, Willlumsen L, et al. High incidence of cortical spreading depression in patients with intracerebral haematomas. Society for Neuroscience Annual Meeting 2008. Society for Neuroscience. 810.2. 2008.

Feuerstein D, Manning A, Hashemi P, Bhatia R, Fabricius M, Pahl C, et al. Dynamic metabolic response to multiple spreading depolarisations in patients with acute head injury: an online microdialysis study. J Cereb Blood Flow Metab 2010. Advance access published on February 10, 2010, doi:10.1038/jcbfm.2010.17.

Gursoy-Ozdemir Y, Qiu J, Matsuoka N, Bolay H, Bermpohl D, Jin H, et al. Cortical spreading depression activates and upregulates MMP-9. J Clin Invest 2004; 113: 1447–55.

Hacke W, Schwab S, Horn M, Spranger M, De Georgia M, von Kummer R. 'Malignant' middle cerebral artery territory infarction: clinical course and prognostic signs. Arch Neurol 1996; 53: 309–15.

Hansen AJ, Quistorff B, Gjedde A. Relationship between local changes in cortical blood flow and extracellular K+ during spreading depression. Acta Physiol Scand 1980; 109: 1–6.

Hartings JA, Strong AJ, Fabricius M, Manning A, Bhatia R, Dreier JP, et al. Spreading depolarizations and late secondary insults after traumatic brain injury. J Neurotrauma 2009; 26: 1857–66.

Hashemi P, Bhatia R, Nakamura H, Dreier JP, Graf R, Strong AJ, et al. Persisting depletion of brain glucose following cortical spreading depression, despite apparent hyperaemia: evidence for risk of an adverse effect of Leao's spreading depression. J Cereb Blood Flow Metab 2009; 29: 166–75.

Heiss WD, Graf R, Wienhard K, Lottgen J, Saito R, Fujita T, et al. Dynamic penumbra demonstrated by sequential multitracer PET after middle cerebral artery occlusion in cats. J Cereb Blood Flow Metab 1994; 14: 892–902.

Hopwood SE, Parkin MC, Bezzina EL, Boutelle MG, Strong AJ. Transient changes in cortical glucose and lactate levels associated with peri-infarct depolarisations, studied with rapid-sampling microdialysis. J Cereb Blood Flow Metab 2005; 25: 391–401.

Hossmann KA. Periinfarct depolarizations. Cerebrovasc Brain Metab Rev 1996; 8: 195–208.

Iadecola C. Bleeding in the brain: killer waves of depolarization in subarachnoid bleed. Nat Med 2009; 15: 1131–2.

Jander S, Schroeter M, Peters O, Witte OW, Stoll G. Cortical spreading depression induces proinflammatory cytokine gene expression in the rat brain. J Cereb Blood Flow Metab 2001; 21: 218–25.

Kobayashi S, Harris VA, Welsh FA. Spreading depression induces tolerance of cortical neurons to ischemia in rat brain. J Cereb Blood Flow Metab 1995; 15: 721–7.

Kudo C, Nozari A, Moskowitz MA, Ayata C. The impact of anesthetics and hyperoxia on cortical spreading depression. Exp Neurol 2008; 212: 201–6.

Kunz A, Park L, Abe T, Gallo EF, Anrather J, Zhou P, et al. Neurovascular protection by ischemic tolerance: role of nitric oxide and reactive oxygen species. J Neurosci 2007; 27: 7083–93.

Lauritzen M, Jorgensen MB, Diemer NH, Gjedde A, Hansen AJ. Persistent oligemia of rat cerebral cortex in the wake of spreading depression. Ann Neurol 1982; 12: 469–74.

Leão AAP. Pial circulation and spreading depression of activity in cerebral cortex. J Neurophysiol 1944a; 7: 391–6.

Leão AAP. Spreading depression of activity in the cerebral cortex. J Neurophysiol 1944b; 7: 359–90.

Leão APP. Further observation on the spreading depression of activity in the cerebral cortex. J Neurophysiol 1947; 10: 409–14.

Martins-Ferreira H, De Oliveira Castro G, Struchiner CJ, Rodrigues PS. Circling spreading depression in isolated chick retina. J Neurophysiol 1974; 37: 773–84.

Mies G, Iijima T, Hossmann KA. Correlation between peri-infarct DC shifts and ischaemic neuronal damage in rat. Neuroreport 1993; 4: 709–11.

Murgatroyd FD, Krahn AD. Handbook of cardiac electrophysiology: a practical guide to invasive EP studies and Catheter ablation. London: ReMedica; 2002. p. 60–4.

Nedergaard M, Astrup J. Infarct rim: effect of hyperglycemia on direct current potential and [14C]2-deoxyglucose phosphorylation. J Cereb Blood Flow Metab 1986; 6: 607–15.

Nedergaard M, Hansen AJ. Characterization of cortical depolarizations evoked in focal cerebral ischemia. J Cereb Blood Flow Metab 1993; 13: 568–74.

Oddo M, Schmidt JM, Mayer SA, Chiolero RL. Glucose control after severe brain injury. Curr Opin Clin Nutr Metab Care 2008; 11: 134–9.

Ohta K, Graf R, Rosner G, Heiss WD. Profiles of cortical tissue depolarization in cat focal cerebral ischemia in relation to calcium ion homeostasis and nitric oxide production. J Cereb Blood Flow Metab 1997; 17: 1170–81.

Park CK, Nehls DG, Graham DI, Teasdale GM, McCulloch J. Focal cerebral ischaemia in the cat: treatment with the glutamate antagonist MK-801 after induction of ischaemia. J Cereb Blood Flow Metab 1988; 8: 757–62.

Petzold GC, Haack S, von Bohlen Und Halbach O, Priller J, Lehmann TN, Heinemann U, et al. Nitric oxide modulates spreading depolarization threshold in the human and rodent cortex. Stroke 2008; 39: 1292–9.

Petzold GC, Scheibe F, Braun JS, Freyer D, Priller J, Dirnagl U, et al. Nitric oxide modulates calcium entry through P/Q-type calcium channels and N-methyl-D-aspartate receptors in rat cortical neurons. Brain Res 2005; 1063: 9–14.

Richter F, Rupprecht S, Lehmenkuhler A, Schaible HG. Spreading depression can be elicited in brain stem of immature but not adult rats. J Neurophysiol 2003; 90: 2163–70.

Sakowitz OW, Kiening KL, Krajewski KL, Sarrafzadeh AS, Fabricius M, Strong AJ, et al. Preliminary evidence that ketamine inhibits spreading depolarizations in acute human brain injury. Stroke 2009; 40: e519–22.

Sharp FR, Lu A, Tang Y, Millhorn DE. Multiple molecular penumbras after focal cerebral ischemia. J Cereb Blood Flow Metab 2000; 20: 1011–32.

Shibata M, Bures J. Reverberation of cortical spreading depression along closed-loop pathways in rat cerebral cortex. J Neurophysiol 1972; 35: 381–8.

Shin HK, Dunn AK, Jones PB, Boas DA, Moskowitz MA, Ayata C. Vasoconstrictive neurovascular coupling during focal ischemic depolarizations. J Cereb Blood Flow Metab 2006; 26: 1018–30.

Somjen GG. Ions in the brain: normal function, seizures, and stroke. USA: Oxford University Press; 2004.

Sramka M, Brozek G, Bures J, Nadvornik P. Functional ablation by spreading depression: possible use in human stereotactic neurosurgery. Appl Neurophysiol 1977; 40: 48–61.

Strong AJ. The management of plasma glucose in acute cerebral ischaemia and traumatic brain injury: more research needed. Intensive Care Med 2008; 34: 1169–72.

Strong AJ, Anderson PJ, Watts HR, Virley DJ, Lloyd A, Irving EA, et al. Peri-infarct depolarizations lead to loss of perfusion in ischaemic gyrencephalic cerebral cortex. Brain 2007; 130: 995–1008.

Strong AJ, Bezzina EL, Anderson PJ, Boutelle MG, Hopwood SE, Dunn AK. Evaluation of laser speckle flowmetry for imaging cortical perfusion in experimental stroke studies: quantitation of perfusion and detection of peri-infarct depolarisations. J Cereb Blood Flow Metab 2006; 26: 645–53.

Strong AJ, Boutelle MG, Vespa PM, Bullock MR, Bhatia R, Hashemi P. Treatment of critical care patients with substantial acute ischemic or traumatic brain injury. Crit Care Med 2005; 33: 2147–9; author reply 2149.

Strong AJ, Harland SP, Meldrum BS, Whittington DJ. The use of in vivo fluorescence image sequences to indicate the occurrence and propagation of transient focal depolarizations in cerebral ischemia. J Cereb Blood Flow Metab 1996; 16: 367–77.

Symon L, Pasztor E, Branston NM. The distribution and density of reduced cerebral blood flow following acute middle cerebral artery occlusion: an experimental study by the technique of hydrogen clearance in baboons. Stroke 1974; 5: 355–64.

Takano K, Latour LL, Formato JE, Carano RA, Helmer KG, Hasegawa Y, et al. The role of spreading depression in focal ischemia evaluated by diffusion mapping. Ann Neurol 1996; 39: 308–18.

Tomlinson FH, Anderson RE, Meyer FB. Acidic foci within the ischemic penumbra of the New Zealand white rabbit. Stroke 1993; 24: 2030–9; discussion 2040.

Umegaki M, Sanada Y, Waerzeggers Y, Rosner G, Yoshimine T, Heiss WD, et al. Peri-infarct depolarizations reveal penumbra-like conditions in striatum. J Neurosci 2005; 25: 1387–94.

Vespa PM, McArthur D, O'Phelan K, Glenn T, Etchepare M, Kelly D, et al. Persistently low extracellular glucose correlates with poor outcome 6 months after human traumatic brain injury despite a lack of increased lactate: a microdialysis study. J Cereb Blood Flow Metab 2003; 23: 865–77.

Yanamoto H, Miyamoto S, Tohnai N, Nagata I, Xue JH, Nakano Y, et al. Induced spreading depression activates persistent neurogenesis in the subventricular zone, generating cells with markers for divided and early committed neurons in the caudate putamen and cortex. Stroke 2005; 36: 1544–50.